Earth and Planetary Science Letters 584 (2022) 117511

Contents lists available at ScienceDirect

Earth and Planetary Science Letters

www.elsevier.com/locate/epsl

Scaling properties of seismicity and faulting

Davide Zaccagnino [a,c,*], Luciano Telesca [b], Carlo Doglioni [c,d]

[a] Earth Sciences Department, Sapienza University, Rome, 00185, Italy
[b] Institute of Methodologies for Environmental Analysis, National Research Council (CNR-IMAA), Tito Scalo (PZ), 85050, Italy
[c] Physics Department, Sapienza University, Rome, 00185, Italy
[d] Istituto Nazionale di Geofisica e Vulcanologia (INGV), Rome, 00143, Italy

ARTICLE INFO

Article history:
Received 15 November 2021
Received in revised form 14 March 2022
Accepted 18 March 2022
Available online xxxx
Editor: H. Thybo

Keywords:
Gutenberg–Richter distribution
Omori–Utsu law
tectonic setting
earthquake triggering
fracturing and fault disorder

ABSTRACT

The Gutenberg–Richter law and the Omori law are both characterized by a scaling behavior. However, their relation is still an open question. Although several hypotheses have been formulated, a comprehensive geophysical mechanism is still missing to explain the observed variability of the scaling exponents b-value and p-value, e.g., correlating the seismic cycle to statistical seismology and tectonic processes. In this work, a model for describing the size-frequency scaling and the temporal evolution of seismicity is proposed starting from simple assumptions. The parameter describing how the number of earthquakes decreases after a major seismic event, p, turns out to be positively correlated to the exponent of the frequency-size distribution of seismicity, b, and related to tectonics. Our findings suggest that $p \approx \frac{2}{3}(b+1)$. It implies that a relationship between fracturing regimes, "efficiency" of the seismic process, duration of the seismic sequences and geodynamic setting exists, with outstanding potential impact on seismic hazard. On the other hand, the Gutenberg–Richter law simply reflects the tendency of the segments of the Earth's crust to reach mechanical stability via constrained energy-budget optimization. Each perturbation has a probability of growing an earthquake or not, depending on disorder within the fault zone and the energy accumulated in the adjoining volume, mainly controlling the evolution of seismic sequences. The results are consistent with the different energy sources related to the tectonic settings, i.e., gravitational in extensional regimes, having higher b and p values, and generating lower maximum magnitude earthquakes with respect to strike-slip and contractional settings, which are rather fueled by elastic energy, showing lower b and p values, and they may generate higher magnitude events.

1. Introduction

Since the dawn of the modern science of earthquakes, a clear split has risen among theoretical and statistical seismology and tectonics. Classical seismology explains what happens during a few seconds of fault slip following rock breakdown, with the consequent radiation of seismic waves, while statistical seismology describes how seismicity occurs in space and time. Even though they investigate the same subject, differences are so deep that they can be put in relation with each other not without significant effort. Statistical seismology is mainly grounded on two fundamental laws, the Gutenberg–Richter law (Gutenberg and Richter, 1944) and the Omori–Utsu law (Utsu and Ogata, 1995). The Omori–Utsu law describes the time evolution of aftershocks represented by the scaling relation

$$n(t) = \frac{z}{(c+t)^p} \tag{1}$$

where $n(t)$ represents the number of seismic events recorded at time t after the mainshock, z and c are constants and p is a scaling exponent usually falling in the range 0.9–1.5 (Utsu and Ogata, 1995).

The Gutenberg–Richter law identifies the relationship between frequency and magnitude of earthquakes

$$N(\geq M_w) = 10^{a-b(M_w-M_{wc})} \tag{2}$$

where a is the logarithm of the number of earthquakes with moment magnitude M_w larger than the completeness moment magnitude M_{wc}, N represents the number of recorded seismic events larger than M_w, and b is the fundamental scaling parameter defining the frequency-magnitude distribution of the earthquakes. For tectonic earthquakes b usually ranges between 0.7 and 1.2 (Schorlemmer et al., 2005). Few hypotheses have been formulated to explain this scaling behavior, for instance, based on computational simulations (Bak and Tang, 1989), power-law generative

* Corresponding author at: Earth Sciences Department, Sapienza University, Rome, 00185, Italy.
E-mail address: davide.zaccagnino@uniroma1.it (D. Zaccagnino).

https://doi.org/10.1016/j.epsl.2022.117511

models and non-extensive statistical mechanics (Tsallis, 1988). The Gutenberg–Richter law has been thoroughly studied; in particular, great attention has been devoted to detect significant variations of b during the seismic cycle (Gulia et al., 2016) with contrasting and sometimes conflicting results because of different criteria applied in data processing and analysis. Our understanding of the relationship between seismicity and tectonics, grounded on some empirical laws (Wells and Coppersmith, 1994), is still poorly developed. It is known that the b-value of the Gutenberg–Richter law is respectively larger in normal-fault seismicity than in strike-slip and reverse faulting (Schorlemmer et al., 2005), the same mutual relation is also true for the length of ruptures involved during the seismic events (Leonard, 2010). Moreover, extensional tectonic settings are featured by diffuse and developed fracturing and larger fractal dimension of the hypocentral distribution of earthquakes than transcurrent and compressive tectonic regions (Aki, 1981). However, a specific theory for spatial and temporal organization of seismicity is missing and the implementation of models proposed starting from necessary approximations under well specified conditions, must be accurately evaluated before application beyond the subject of conception (Kagan and Jackson, 1991). A first attempt to include seismicity into a clear theoretical physical framework can be found in Bak and Tang (1989), which stated that the brittle crust belongs to the so-called self-organized critical systems (SOC). According to this view, large seismic events occur for the same reasons of smaller ones, the only difference is given by the internal state of stability of the fault system, hence the wide range of possible dynamic evolutions. However, SOC-models are computational tools which can be extremely effective in working out fundamental aspects of seismicity, but they cannot explain the complex pattern of features relating fracture dynamics, statistical properties of seismicity and tectonics in which the role of disorder was proven to be crucial (Goebel et al., 2017). It is likely that the brittle crust belongs to the wide group of physical systems whose turbulent dynamics is strongly controlled by their internal disorder (Boffetta et al., 1999) more than by self-organization and criticality, mainly emerging in limited spatial and temporal windows under specific conditions (Nandan et al., 2021).

2. Theory

In this section we realize simple derivations of the Gutenberg–Richter law and Omori–Utsu law starting from reasonable physical hypotheses. For the sake of readability, a fluent discussion is given hereinafter, while a complete derivation is presented in the Supplementary Material using a certain number of mathematical approximations to reach an analytical result. We are interested in providing a compelling physical mechanism to put in relation the observed variability of the scaling exponents of the power laws with the most important geophysical and tectonic properties, connecting coseismic dynamics to tectonic ones: from simple cracks to complex seismic sequences. Since we aim at achieving a comprehensive framework for seismicity, we provide a derivation in which coseismic and global seismic dynamics are not distinguishable, so that, henceforth, what we write can be interpreted like regarding both a single seismic event and a whole seismic sequence. In fact, earthquakes are not physical entities, but just peaks of seismic activity strongly localized both in space and time. For the sake of simplicity, we use the language of seismic sequences to which the reader is supposed to be more familiar.

2.1. Time evolution of seismicity

In this paragraph, the temporal features of seismic sequences are discussed and a possible derivation of the Omori–Utsu law, assuming the Gutenberg–Richter scaling relation, is proposed. A fault can be described as a thin contact zone separating two contiguous crustal volumes, on which a tectonic stress is applied, briefly represented as an inclined sliding plane with asperities and barriers, friction anisotropies alternating weaker and more competent interfaces respectively with lower and higher static friction, hence more or less prone to breaking. The upper layers of rocks show a brittle behavior up to the depth of the brittle-ductile transition (BDT) and rest on a lower and viscous one. The upper layers slowly slide over it, gradually accumulating deformation. When a low friction area breaks, the fault plane slips on average for a length u_0, partially releasing during the event the stored energy in the adjacent volume. After the earthquake (the peak of the energy drop) has occurred, the two blocks are still not in equilibrium, since the hanging wall volume has not dissipated the whole energy; furthermore, the viscous layer dissipates stress (e.g., Helmstetter and Shaw, 2009) through an exponential relaxation featured by a certain proper relaxation time τ. Therefore, the relative position $u(t)$ between the hanging wall and the footwall can be modeled according to an exponential relaxation. Since the seismic moment M, which measures the energy released during the coseismic rupture, depends linearly on the seismic slip, it is possible to define a cumulative seismic moment $M(t)$, given by the sum of the moments associated with all the events occurred from the time origin of the mainshock $t = 0$ until t within a given volume enclosing the fault zone as $M(t) = \mu A u(t)$, where μ is the shear modulus of the rocks at the interface and $u(t)$ is the mean value of the slip averaged over the fault interface A. If the energy balance of fault relaxation is dominated by seismic nucleation, which can be assumed to be true in the early stages of the post-seismic phase, the relation for the cumulative seismic moment can be linearized, so that, after a certain time interval T needed for stabilization, the current state of the seismic sequence featured by the cumulative moment magnitude $M_w(t) = \frac{2}{3}\log(M(t)) - 6.1$ can be obtained in terms of the total number of seismic events above the completeness magnitude, i.e., the minimum magnitude at which data respect the Gutenberg–Richter law, before time t, $N(t)$:

$$N(t) \simeq N\left[1 - \alpha\left(\frac{\tau}{\mu A \Delta}\right)^{\frac{2}{3}b}(c+t)^{-\frac{2}{3}b}\right] \tag{3}$$

where N is the total number of shocks in the sequence, $\alpha = 10^{6.1b}$, $c = \frac{u_0\tau}{\Delta} - T$, $\Delta = u(T) - u_0$. Then, the number of earthquakes at time t reads

$$n(t) \propto (c+t)^{-p} \tag{4}$$

Eq. (4) not only confirms Utsu's (1961) findings about the decrease of the number of aftershocks with time according to a power-law with scaling exponent p, but also highlights that p is positively correlated to the scaling exponent of the Gutenberg–Richter distribution b, according to

$$p = \frac{2}{3}b + 1 \tag{5}$$

However, this relation is valid under the strict approximations assumed above, which should be relaxed when real seismic sequences are considered. In Section 4, this issue is discussed, achieving the result that the above equality is just an ideal relation, so that, $p \propto b$, but the values of p are smaller than $\frac{2}{3}b + 1$.

2.2. The frequency-magnitude scaling

Now we focus on the links among the Gutenberg–Richter b-value, its fluctuations and the energy balance in faulting. A step-by-step mathematical derivation is provided in the Supplementary

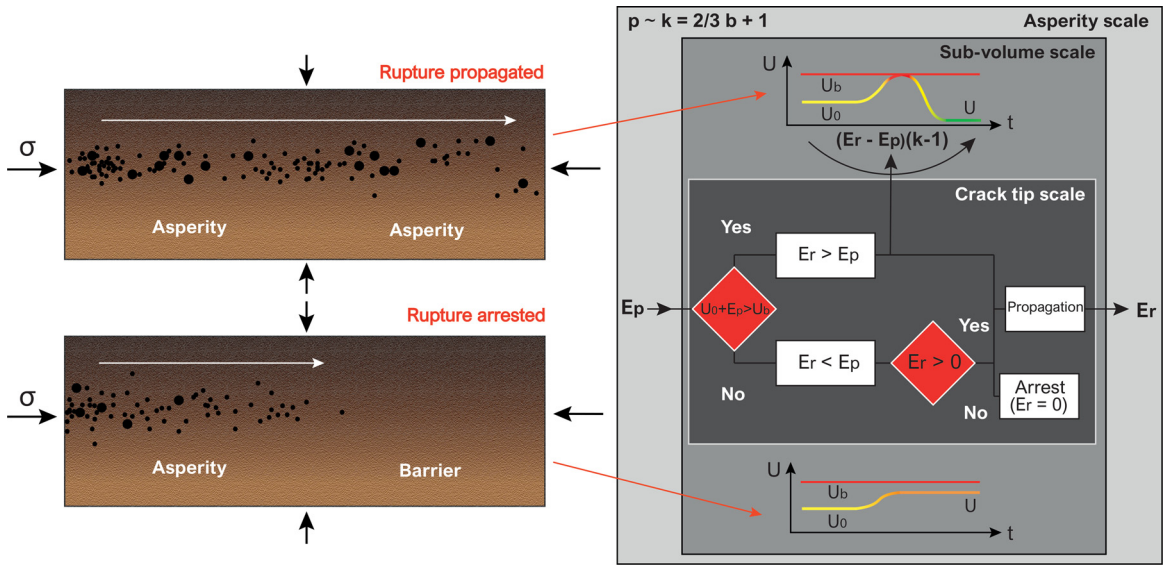

Fig. 1. Graphical representation of earthquake dynamics. On the left, two different stages of fracture dynamics, fracture propagation (top) and fracture arrest (bottom), explained by the picture on the right. A fault interface is divided into several sub-volumes featured by highly correlated stress patterns and seismic behavior. An initial perturbation (E_p) interacts with a segment of the fault interface at the level of a certain sub-volume. Based on its internal stability state, represented by the initial internal energy (U_0), the interface breaks down if the perturbation increases its energy (U) beyond the breakdown level (U_b). In that case, the slip occurs and the fracture spreads rapidly; not only that, since the fault zone is in an unstable and frustrated state, i.e., a configuration forced by tectonic stress (σ), meanwhile the fracture propagates, the sub-volume moves towards a more stable energy level, amplifying energy release by a factor k. Therefore, k is an estimation of the triggering power of fracture within the interface. At large spatial and temporal scales, k is proportional to the exponent of the Omori–Utsu law, p. The perturbation increases up to a final residual value (E_r), ready to be transmitted to the next interface. Conversely, if the critical level of failure U_b is not reached, the segment of the fault plane within the sub-volume becomes more unstable than before and absorbs part of the initial perturbation slowing the propagation of the fracture, i.e., it behaves as a barrier. If the initial disturbance is completely absorbed, then the faulting process stops. Both seismic events and large-scale seismicity optimize this process so that crustal volumes reach a mechanical state of improved stability as soon as stress conditions allow it.

Material. In our model, a fault is thought as a rough interface consisting in a relatively thin rock with respect to its length in which the stress stored during the interseismic period is suddenly released during the coseismic phase. Therefore, faults are passive planes where friction allows or not the delivering of the energy accumulated in the overlying or adjacent crustal volumes. In our model, it is assumed that slip and associated seismicity completely occurs within the fault zone. In order to keep our study as simple as possible, the fault interface is divided into sub-volumes (or segments) featured by highly correlated seismic behavior, so that it is assumed that the latter is not directly influenced by seismicity occurring outside. Once an initial perturbation E_p had interacted with the interface, the weakest segment may break. It happens only if the perturbation brings the internal energy of the interface at the level of the crack-tip beyond its breaking level, causing an energy drop; therefore, the starting perturbation increases up to a new residual value, said E_r, which is now transmitted to the next sub-volume along the fracture path. Moreover, since the fault zone is in an unstable and frustrated state, i.e., a configuration forced by tectonic stress, meanwhile the fracture propagates, the sub-volume moves towards a more stable energy level, amplifying energy release by a factor k. Therefore, k is an estimation of the triggering power of fracture within the interface. The rupture spreads out only if the initial perturbation grows along the path of the crack, which implies $E_p < E_r$. Faulting stops if $E_r = 0$. During the sequence, a large number of seismic events occur. The cumulative seismic moment M can be written in terms of certain probabilities p_i that events of seismic moment M_i can occur, $M = \sum_i M_i p_i$ and, analogously, the total gain energy, defined as the relative variation of the perturbation energy with respect to the starting one, is given by the sum of the contributions which come from each fault segment is $\epsilon = \sum_i \epsilon_i p_i$. It is reasonable that earthquake dynamics evolves such that crustal volumes can be displaced, in order to improve the state of mechanical stability of fault interfaces, by optimizing the total energy gain produced via fault segment breaking. Of course, the optimal solution is constrained by dynamic conditions (Fig. 1). A fixed seismic moment must be nucleated because of approximatively constant strain rates over long time periods. Hence, we suppose that given the dislocation constraint $\overline{M}$, which depends on the deformation rates of local geodynamics, seismicity optimizes the triggering power of crack propagation, so that both seismic sequences, according to the framework we are working with, and single earthquakes are ultimately driven by fault disorder (spatial distribution of barriers and asperities). The constrained optimization procedure, described in detail in the Supplementary material, returns a survivor function, giving the probability that an earthquake can overcome a certain seismic moment, which is well approximated by a power law

$$S(M) \sim \left(\frac{M_c}{M}\right)^{k-1} \tag{6}$$

in the range of seismic moments of our interest. Then, the exponent of the Gutenberg–Richter law is $b = \frac{3}{2}(k-1)$.

2.3. Stress vs fracturing

In this paragraph we deal with the relationships between seismicity and geophysical properties of faulting also connected to the local tectonic settings. We are interested in understanding whether it is possible to connect the conditions of crack growth with the stress patterns typical of different tectonic settings. The simplest way to decide upon the stability of a fracture is to consider, for the sake of simplicity, a crack produced by a load σ acting on a wide plate, and to analyze how its energy balance changes under suitable conditions. In regular earthquakes fault slip velocity is usually three orders of magnitude smaller than rupture speed

(Udías et al., 2014); therefore, the variation of kinetic energy can be neglected at the time scale of crack propagation, so that the critical condition for the growth of the rupture in terms of its length, L, can be written as

$$-\frac{d}{dL}E_e - \frac{d}{dL}E_g = \frac{d}{dL}E_s + \frac{d}{dL}E_d \tag{7}$$

where E_e is the elastic energy, E_g represents the gravitational energy of the failure volume, E_s is the so-called surface energy and E_d is the amount of energy dissipated by friction. The crack is unstable and tends to grow if the rate of change of surface energy is smaller than the variation of potential energy. Fracturing stops when the accumulated stress is no longer sufficient to supply the minimum energy for the formation of fresh surface (Brace, 1960).

In particular, the elastic energy released during the propagation of a shear crack of length L, involving the crust for a thickness D under a stress load σ is $E_e \propto -D\sigma^2 L^2$ (Udías et al., 2014).

The proportionality coefficient considers the elastic properties of rocks (usually the elastic rigidity μ). The surface energy can be evaluated through $E_S = -2\gamma DL$, where γ is the average surface density energy, i.e., the amount of energy released when a unit of surface is produced, while $E_d = -\mu DLu$ is the total amount of energy loss due to friction at fault interface, $u_{max} \sim cL$ (Scholz et al., 1993) is the average fault slip and $c \approx 0.001$.

The variation of gravitational potential energy can be written in terms of the average vertical displacement as $\frac{d}{dL}E_g = \pm DR\rho gu\sin\xi$, where $-$ is chosen in normal faulting and $+$ in reverse faults, ξ is the angle of dip of the fault. So, we find

$$\sigma(L,u) \approx \sqrt{\frac{\mu(2\gamma + \mu u \pm R\rho gu\sin\xi)}{2\pi(1-\nu)L}}, \tag{8}$$

where ρ is the average value of density of the rocks of the failure volume and ν is the Poisson's modulus. As a next step, we should consider that earthquakes occur in multifractal clusters (Turcotte, 1989; Chelidze et al., 2018). In this regard we can define and locally measure the fractal dimension of the earthquake sequence so that the critical surface at the resolution scale s behaves like if the dislocated surface $\Sigma_c(s) \sim s^{-D_f}$, where D_f is the fractal, box-counting dimension.

Taking as a reference an ideal planar faulting with fractal dimension $D_f^{(0)} = 2$, if Σ_0 is the surface produced to dissipate a certain amount of energy stored in the crust, then, for a generic fault

$$\Sigma_c(s) \propto \left(s^{D_f^{(0)} - D_f}\right)\Sigma_0 \tag{9}$$

The fractal dimension of earthquakes has long been the subject of several studies (e.g., Kagan and Jackson, 1991); to date, the generally accepted value (Goltz, 1997) for large-scale faulting is $D_f = 2.20 \pm 0.05$. However, a wide variability has been found, partially due to the unmodeled heterogeneity of the data (Kagan, 1993). Nevertheless, it seems clear that a substantial difference exists in fractal dimensions between compressive and extensional faults (e.g., Hirata, 1989) and between deep and intermediate earthquakes (Goltz, 1997).

The fractal dimension of a pattern of seismic hypocenters depends on the topological properties of the fault systems: an ideal, perfectly flat fault is two-dimensional; complexities promote the development of rough interfaces. Therefore, a quick estimate of roughness and fractal dimension can be made through the evaluation of energy available for dissipation during the seismic process. Given our results presented in the previous section, we can write that

$$D_f \propto \frac{2}{3}b \tag{10}$$

Table 1
Features of the main seismicity in Italy in the last three decades. For each seismic sequence, p values of the Omori–Utsu laws are listed in the sixth column. Each power law scaling starts after a major seismic event whose timing is in the second column, while its epicentral coordinates and moment magnitude are, respectively, in the third, fourth and fifth columns.

Name seismic sequence	Date	Epicenter		M_w	p-value $\pm\sigma_p$
		Latitude	Longitude		
Colfiorito	26/09/1997	43.014	12.853	6.0	1.53 ± 0.01
	03/10/1997	43.042	12.824	5.2	1.24 ± 0.01
	14/10/1997	42.898	12.898	5.6	1.29 ± 0.02
	26/03/1998	43.145	12.809	5.3	1.20 ± 0.04
L'Aquila	06/04/2009	42.342	13.510	6.3	1.69 ± 0.02
	22/06/2009	42.445	13.354	4.7	1.94 ± 0.09
Emilia	20/05/2012	44.895	11.263	6.1	1.57 ± 0.03
	29/05/2012	44.841	11.065	5.9	1.34 ± 0.02
Central Italy	24/08/2016	42.698	13.233	6.0	1.11 ± 0.02
	26/10/2016	42.904	13.090	5.9	1.59 ± 0.08
	30/10/2016	42.830	13.109	6.5	1.18 ± 0.02
	18/01/2017	42.531	13.283	5.5	1.09 ± 0.03

This is in excellent agreement with both the classical result $D_f = 3\beta$, where $\beta = 2b/3$ (Aki, 1981) and observations; in particular, normal faulting is featured by $D_f \sim 2.2$–2.7, strike-slip faulting has $D_f \sim 1.9$–2.3, while $D_f \sim 1.5$–2.0 in reverse faulting.

This means that various fracturing regimes occur because of different tectonic settings, which change the critical stress required for rupture propagation. Unlike contractional and strike-slip tectonic settings, extensional tectonic regimes determine a more diffuse interseismic dilatance within the brittle crust, resulting in widespread fracturing. Extensional tectonic settings have in average lower maximum magnitude, shorter fault length and smaller coseismic slip with respect to other tectonic settings (Doglioni et al., 2015a). These observations, which are discussed in the next section, follow immediately from the classical structural relationships between properties of earthquakes scaling and faulting.

3. Application to Italian seismicity

We analyze the four largest seismic sequences that struck Italy in the last decades, three related to extensional tectonics (1997 Colfiorito, M_w 6.0; 2009 L'Aquila, M_w 6.3; 2016 Amatrice-Norcia, M_w 6.5) and one to a compressive setting (2012 Emilia, M_w 6.1) as examples of how the exponent of the Omori–Utsu law p relates with the instability of the crustal volumes. Of course, a statistical analysis must be performed using several dozens of seismic sequences characterized by multiple large earthquakes to prove our hypothesis. In the present work, the cumulative number of earthquakes during a seismic sequence with magnitude higher than M_{wc} is fitted by using the following Omori–Utsu cumulative function (Ogata, 1983)

$$N(t) = \sum_{k=1}^{K} \frac{g_k}{1-p_k}(t - t_k + c_k)^{-(p_k-1)}H(t-t_k) \tag{11}$$

where g_k is a fit parameter proportional to the number of earthquakes occurred at t_k, i.e., the timing of the k-th main earthquake, $t - t_k$ is the time past from the k-th large event and $H(t-t_k)$ denotes the step function relative to the k-th Omori–Utsu law. The fitting function (11) involves the sum of K Omori–Utsu laws, each one with scaling exponents p_k; K is chosen as minimal but enough to guarantee a good fit.

Table 1 and Fig. 2A show the results relating to the seismic sequence generated by the extensional tectonics that shook Umbria and Marche from 26th September 1997 until the following spring

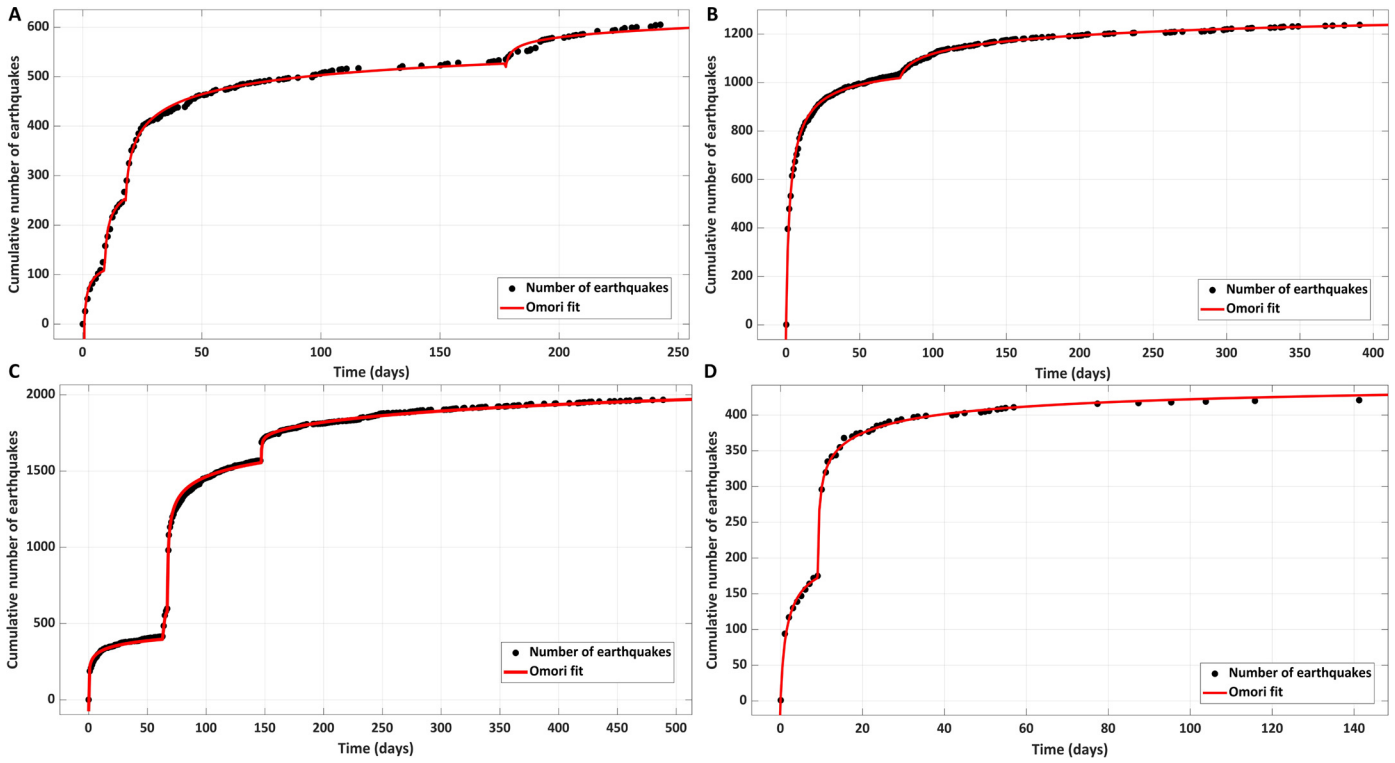

Fig. 2. Aftershock sequences temporal evolution analyzed by using multiple Omori–Utsu laws fit given by the following formula $N(t) = \sum_{k=1}^{K} \frac{g_k}{1-p_k}(t - t_k + c_k)^{-(p_k-1)} H(t - t_k)$ for four seismic sequences in Italy: (A) Cumulative seismicity in Umbria (only events of ML > 3.0 are considered), Colfiorito sequence, started on 26th September 1997 with the extensional M_w 6.0 mainshock and aftershocks. Fit $R^2 = 0.97$. Four Omori's laws are applied to achieve this result, in fact if a lower number of power laws was used, the fit quality would be lower (e.g., $R^2 = 0.77$ for $K = 1$, $R^2 = 0.93$ for $K = 2$ and $R^2 = 0.94$ for $K = 3$). (B) Cumulative seismicity in Abruzzo (ML > 2.4), after the April 6th, 2009, extensional M_w 6.3 mainshock. Fit $R^2 > 0.99$. (C) Cumulative seismicity in Central Italy (ML > 2.7), started with the extensional August 24th, 2016, M_w 6.0 Amatrice earthquake and the following October 30th M_w 6.5 Norcia mainshock. Fit $R^2 > 0.99$. (D) Cumulative seismicity in Emilia (ML > 2.8), 2012 started with the compressive May 20th M_w 6.1 earthquake. Fit $R^2 > 0.99$.

(Amato et al., 1998), causing considerable damage to the artistic heritage and buildings in several villages and towns such as Assisi and Preci. In this case, the parameter p took its maximum value just after the mainshock (26th September 1997, M_w 6.0, with M_w 5.6 foreshock four hours earlier) and then progressively decreased: it is a clear sign that the fault system was slowly stabilizing. The measured trend for p turns out to be compatible with the theoretical prediction proposed above.

Different conclusions are obtained for the normal fault-related seismic sequence of L'Aquila (Scognamiglio et al., 2010), in which the destructive M_w 6.3 earthquake of 6th April 2009 was followed by a lot of smaller aftershocks. Our results are shown in Fig. 2B. In this case, the p value increases significantly, which suggests that seismic nucleation was continuing fast at the end of the L'Aquila seismic sequence. In particular, the number of earthquakes remained significant with respect to the seismic activity occurred before the M_w 6.3 event to north of the sequence fixed the completeness magnitude even after the seismic sequence ended in 2012. It may suggest that faults were still in a metastable state that was slowly evolving towards major destabilization, i.e., the Amatrice-Visso-Norcia seismic sequence. On this regard, during the 2016–2017 normal faulting related seismic sequence of Central Italy (Chiaraluce et al., 2017) (Fig. 3), the parameter p followed a more complex trend. After the M_w 6.0 earthquake of 24th August 2016, which devastated Accumuli, Amatrice and their surroundings, Omori–Utsu law shows a slow dissipation rate ($p \sim 1.11$, Table 1) with the estimate for p (Fig. 2C, Table 1). After the two earthquakes of 26th October 2016, the Apennine crust reaches its maximum instability, evidenced by the rise of the Omori scaling parameter ($p \sim 1.59$), which leads to the M_w 6.5 earthquake of 30th October 2016. This event massively contributed to the release of the still trapped energy in the hanging wall, which is why the p value decreased rapidly (Table 1).

We also analyzed the earthquakes that hit Emilia in 2012 (Ventura and Di Giovambattista, 2013) with two mainshocks (20th May, M_w 6.1; 29th May, M_w 5.9), we reached the same conclusions as the sequences discussed above (Fig. 2D).

These results put in evidence that a link between p, which is proportional to the triggering capacity of the strongest seismic events, and the instability of fault systems, could exist. High p values are connected to rapid mechanical stabilization, while low ones indicate slow triggering power. Results in good agreement with our interpretation are also reported in recent works (e.g., Shcherbakov, 2021). However, the interpretation of such data is not unambiguous: a slow triggering Omori relaxation may both be accompanied by intense aseismic slip due to fault lubrification or be the signal of a still partially locked fault system, where the first broken segment is surrounded by barriers which do not allow a more generalized dislocation. On the other hand, elevated p values could be suggestive of efficient seismic triggering with fast decrease of seismic activity, but, since they are just instantaneous parameters, no mathematical relation ensures us that an additional fault segment activation may occur in the near future. Once more time, the role of disorder within the fault zone is crucial for the dynamical evolution of seismicity.

4. Results and discussion

In the previous sections we introduce the theoretical framework, now we discuss several results concerning the statistical properties of seismicity and their connections with the tectonic environment.

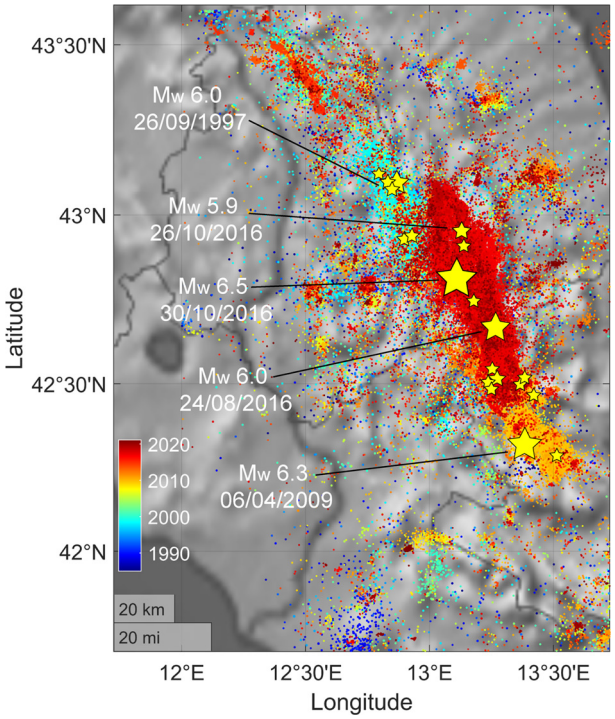

Fig. 3. Seismicity in Central Italy from 1985 to 2021. Light blue points represent earthquakes related to the Colfiorito seismic sequence (1997–1999), yellow and orange ones refer to seismic events happened from 2009 until 2015, while red circles mark the seismic sequence started in 2016. The yellow stars stand for the events with magnitude larger than 5.0. (For interpretation of the colors in the figure(s), the reader is referred to the web version of this article.)

4.1. How are b and p related to each other?

Our results described in Section 2 clearly suggest that b and p are positively correlated. However, they have been derived starting from strict approximations, therefore, it is now necessary to underline some issues:

- The obtained proportionality constant in (4), $z = (p-1)N\alpha \times (\frac{\tau}{\mu A \Delta})^{\frac{2}{3}b}$ depends on the magnitude of the mainshock through the displaced fault surface A, on the slip due to post-seismic sliding and on the p-value itself.
- $c = \frac{u_0 \tau}{\Delta} - T \lesssim O(1)$ is no more a simple constant without a clear physical meaning, but it is directly proportional to the stabilization time τ of the fault.
- p is positive because $b \approx 1$; in particular, since generally the range of variability for b is $0.6 \leq b \leq 1.3$, according to Eq. (4), p should vary between 1.3 and 1.8 at equilibrium.
- However, p is a non-equilibrium parameter with a very simple physical interpretation: it is proportional to the speed of energy release (Dieterich, 1994), and it provides a measure of how much the perturbation induced by the mainshock triggers destabilization in the surrounding volumes.
- The relation between b and p is obtained for $t \ll T$, this means that $p = 1 + \frac{2}{3}b$ is a correct estimate of the parameter just after the mainshock occurs, then it cannot be considered reliable, while p can assume any value in the range $p \leq 1 + \frac{2}{3}b$. Compare it with Fig. 2, Table 1 and with Section 2.2, where the equilibrium condition is equivalent to have independent seismic clusters within the fault segments, i.e., there are not first order aftershocks of earthquakes occurred outside the cluster itself – so that the joint probability of clusters is simply the product of marginal probabilities.
- Since the maximum instability is generally reached at the time of the mainshock, in the post-seismic phase the value of p is expected to decrease if other fault segments are not activated (compare with our results in Section 3).
- Previous remarks suggest that p may be a useful parameter to discern whether the mainshock of an evolving seismic sequence is still pending under the conditions and limitations listed at the end of the previous section. In fact, this can happen whenever the perturbation generated by a seismic event is amplified in the surrounding faults; however, further investigations are required to better understand this issue.
- Our work is not the first concerning the relation between p and b (e.g., Utsu, 1961; Wang, 1994; Guo and Ogata, 1997; Helmstetter and Sornette, 2002). In the previous literature different and sometimes contrasting results exist. For instance, in Wang, 1994, a negative correlation between b and p value is found for a selection of 51 major earthquakes, while Guo and Ogata, 1997 asserted a direct correlation between b and p by analysing a set of about thirty seismic events. That result was in good agreement with the theory provided by Utsu in 1961, according to which $p = 4/3\ b$. In Helmstetter and Sornette, 2002, is instead showed that, using bifurcation theory, the Omori scaling exponent can be written in the form $p = 1 + \theta$, where theta is a small parameter which can also be negative. Our results are compatible with the last three articles: it can be noticed that, since $b \sim 1$, $p = 4/3b \approx 2/3(b+1)$, which is in excellent agreement with the fit in Fig. 4. This means that our model correctly provides for the correlation coefficient between p and b, with the great advantage of connecting its variability to the whole spectrum of geological and geophysical properties of faulting in a simple way. However, it is not able to give us the exact value of the exponent. The difference between the resulting equation of our fit in Fig. 4 and the equation $p = 1 + \frac{2}{3}b$ is a positive shift ultimately caused by the partial failure of our starting hypothesis of independence of seismic activity belonging to different sub-volumes (compare with Section 2 and Supplementary material), so that Eq. (5) should be thought as an upper limit for p once b had been fixed, as already discussed, while the right value of the Omori–Utsu scaling exponent is given by $p = 1 + \theta$, where $\theta \approx \frac{2b-1}{3}$, which is in agreement with Helmstetter and Sornette, 2002.
- Since k controls the amplification of the initial perturbation in $E_r = E_p(\frac{e}{k} + 1)$, comparing the exponent in Eq. (6) with b, $l := k - 1 = \frac{2}{3}b$ can be interpreted as a term of dissipation. This result relates the scale parameter of the frequency-magnitude distribution to the fraction of energy that is dissipated in several different correlated phenomena. More specifically, it states that in reverse faulting, where fracturing is less widespread, a larger fraction of the energy generates stress drop, on the contrary, in extensional faults, where fracturing is extremely developed, dissipation dominates the energy balance, suppressing the probability of extreme events. It is coherent with our results in Section 2.3 about the fractal dimension of hypocentral patterns. All this is extremely consistent with geophysical observations. The geophysical meaning is that, neglecting fluctuations, in subduction zones and mountain ranges about 40–55% of the released energy contributes to stress drop, whereas the residual part is dissipated by shear heating, fracturing and folding of rocks and seismic waves radiation. In extensional tectonic settings, on the other hand, the stress drop is more reduced (25–40%) due to a larger dissipative contribution, which reflects an extremely packed faulting with widespread fracturing. This increases the likelihood of strong secondary seismic events (which is also coherent with larger b-values, e.g., Amato et al., 1998; Daniel et al., 2008)

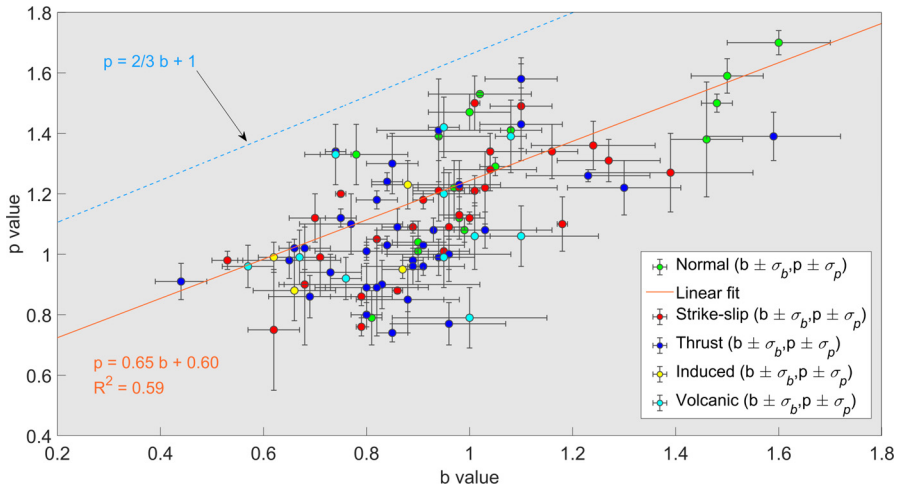

Fig. 4. Scatterplot of p versus b. p value and b value are positively correlated according to the result of the linear fit plotted above. A selection of one hundred seismic sequences among the most investigated in the last decades is given. Each circle represents a seismic sequence, and its color allows to recognize the tectonic setting where it occurred: extensional faulting is painted in green, blue is used for subduction and thrust events, red for strike-slip ones, while fluid injection-induced sequences are in yellow and volcanic-tectonic sequences are cyan dyed. Further information is provided in the Supplementary Material, Table S2. As expected, all the dots are out of the forbidden half-plane bounded below by the line of equation $p = 1 + \frac{2}{3}b$. The best weighted linear fit returns $p = 0.60 + 0.65b$.

and longer duration of seismic sequences in normal fault systems. Our results are compatible with classical and up-to-date scientific literature (Brune's model gives an efficiency of 44%, Brune, 1970).

- When an asperity breaks, surrounding volumes are affected by a positive energy shift because the potential barrier due to the removed roughness has been lowered. Then l can be interpreted as an energy term promoting instability within the fault zone (compare with Fig. 2 and Section 2.2). Its modulus equals the dissipated fraction of the budget required for fault activation and asperities breaking. Moreover, we notice that, at equilibrium, $k = p$, where p is the parameter of the Omori's law. Therefore, k represents the triggering power of the initial perturbation depending on the instability of local asperities. Thus, any stress perturbation over a fault has some chance to become a ruinous earthquake depending on the topology of the fault system, on its previous state of stress and the amplitude of the triggering perturbation. Therefore, seismicity can be understood on the light of disordered, self-organized and critical systems, so that earthquakes turn out to share some peculiar features with the celebrated Bak's sandpiles (Bak and Tang, 1989). Hence, they do not require a well-determined storage of elastic energy to occur, since a lot of sources of complexity mainly control the dynamic evolution of fault systems down to the smallest detail, whatever the energy accumulated. This is consistent with the strong clustering of seismic sequences at both short and long timescales (Kagan and Jackson, 1991; Salditch et al., 2020), and with iterated ruptures (Stein et al., 2012). These results strengthen our belief that long-term seismic dynamics in fault systems is mainly driven by topological disorder and mechanical triggering as suggested, for instance, in Gabrielov et al., 1996, and not by friction and elastic energy accumulation and release, which, on the contrary, play their role at coseismic timescale, when seismic waves are radiated.

4.2. Seismicity vs tectonics

The b-value tends to be 1.0 at the global scale, indicating that the energy accumulation and dissipation throughout seismicity occurs for the whole Earth. However, at the planet scale, the b-value varies as a function of the tectonic style, i.e., 1.10–1.15 for extensional tectonic settings, ~ 1.0 for strike-slip environments, and 0.7–0.9 for contractional earthquakes (Schorlemmer et al., 2005). In fact, normal faults in continental regions generate maximum lower magnitude events around M_w 7.5, much lower than thrusts, which can reach M_w 9.5. The increase of magnitude implies growing volumes and bigger faults moving from extensional to contractional earthquakes, as suggested by Doglioni et al. (2015a). This variability has been attributed either to the lower strength of the continental lithosphere (Neely and Stein, 2021), or to the different mechanisms playing a relevant role at tectonic and geodynamic timescales, e.g., gravitational in extensional tectonic settings and elastic in transcurrent and contractional tectonic settings (Doglioni et al., 2015a,b). In fact, at a given magnitude, normal faults-related earthquakes have more numerous aftershocks that also last longer because they move in favor of gravity (e.g., Valerio et al., 2017). On the contrary, thrusts have volumes moving against gravity, hence loosing quicker the energy to move upward the fault hanging wall and smaller number and shorter duration of aftershocks. However, regardless the tectonic style, at the local scale, the b-value can be extremely variable (e.g., 0.5–1.6) due to regional tectonics, rheology and strain rate and what really matters for seismic hazard assessment is the regional b-value. The most popular model inversely relates the value of b to the tectonic stress in the rock volume surrounding the fault plane (Petruccelli et al., 2019).

Our theoretical results, briefly illustrated in Section 2, prove that various fracturing regimes occur because of different tectonic settings, which change the critical stress needed for fracturing, Eq. (8), and then the parameters of the size-frequency distribution and the temporal evolution of local seismicity vary (Eq. (6)). This effect results in widespread fracturing in extensional tectonic environment (e.g., grabens, pull-apart basins etc.) because $\Sigma_{ext} > \Sigma_0$ (compare with Eq. (9) and Eq. (10)), so that potential energy is efficiently dissipated over a broad range of scales, implying higher probability of secondary rupture and the possibility of longer aftershocks duration in extensional tectonic settings.

On the contrary, subduction zones and thrust-associated faulting show surface fractures with $\Sigma_{compr} < \Sigma_0$, which requires gathered rifting and foster concentrated stress drop (e.g., in agreement with Allmann and Shearer, 2009).

Moreover, Eq. (8) has another straightforward outcome: normal events can be triggered by weaker stress perturbations than those needed for reverse faulting (Zaccagnino et al., 2020). This property justifies why normal fault quakes are found to correlate stronger than reverse fault seismicity with tidal stress modulations (Zaccagnino et al., 2021). The energy conditions are instead stricter

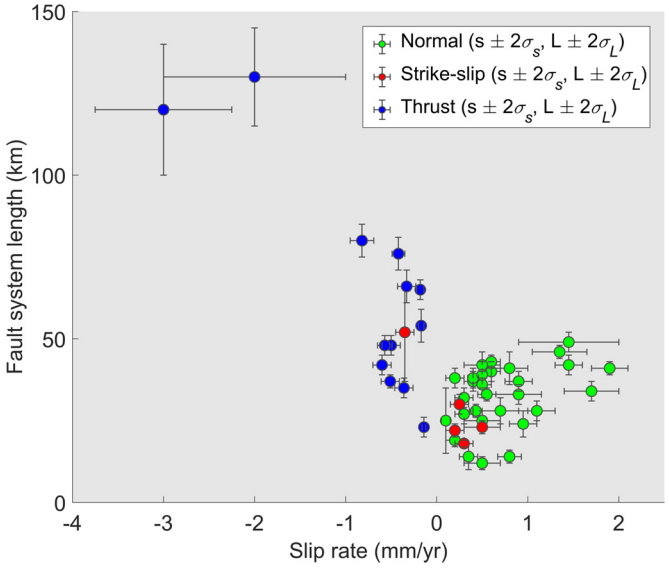

Fig. 5. Scatterplot of the length of faulting versus the annual slip rate in different tectonic settings. Extensional faults (green circles) are featured by lower length along strike with respect to compressive faulting (blue dots) once the average modulus of the slip rate is fixed. Strike-slip faults are highlighted in red. In this plot 47 fault systems in Italy are considered, according to the ITHACA database (ITHACA Working Group, 2019) and previous literature. Further references and description are in the Supplementary material.

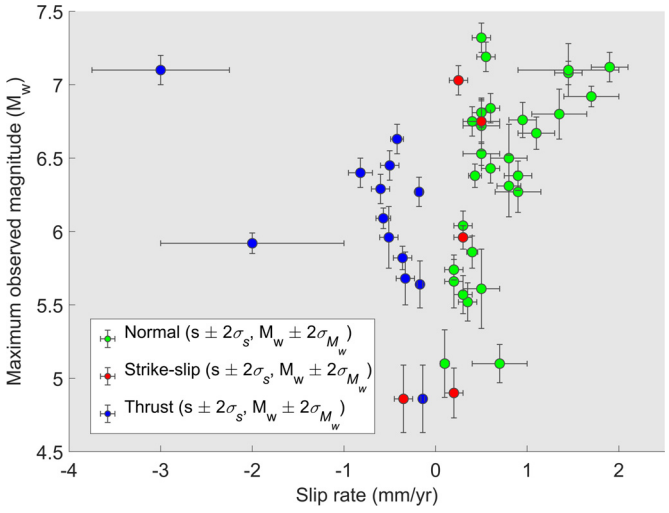

Fig. 6. Scatterplot of the maximum recorded magnitude versus the annual slip rate. Extensional faulting (green dots) and compressive tectonic settings (blue circles) are prone to extreme events with similar magnitudes where the deformation rates are the same. This picture benefited of the data contained in the CPTI15 catalogue of historical seismic events occurred in Italy since the XI century (Rovida et al., 2020).

for events occurring in a compressive tectonic setting, so it is reasonable to expect that they correlate very little with the intensity of tiny perturbations, e.g., tidal stress (Cochran et al., 2004).

As stated in Section 2.3, substantial difference exists in fractal dimensions between compressive and extensional faults and between deep and intermediate earthquakes: $D_f \sim 2.2$–2.7 for normal faulting, $D_f \sim 2.1$–2.3 in strike-slip faulting while $D_f \sim 1.5$–2.0 in reverse faulting.

This effect results, coherently with our sentences above, in widespread fracturing in extensional tectonic environment (e.g., grabens, pull-apart basins etc.) because $\Sigma_{ext} > \Sigma_0$ according to Eq. (10). Then, fixed the seismic moment M, the average slip $u_{ext} < u_0$ and the fractured fault length $L_{ext} < L_0$. On the contrary, subduction zones and thrust-associated faulting show surface fractures $\Sigma_{compr} < \Sigma_0$, which implies $u_{compr} > u_0$ and $L_{compr} > L_0$.

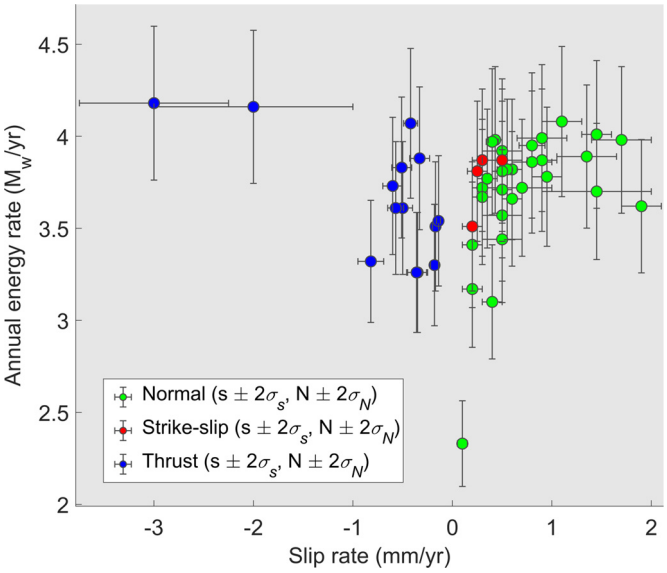

Fig. 7. Scatterplot of the annual seismic energy rate versus average slip rate. Compressive and extensional faults in Italy nucleate equivalent seismic energy expressed in moment magnitude with the same slip rate during interseismic periods. The annual energy rates are calculated by adding the seismic moments of the events occurred within a volume embedding the considered fault system. Further explanations are given in the supplementary material.

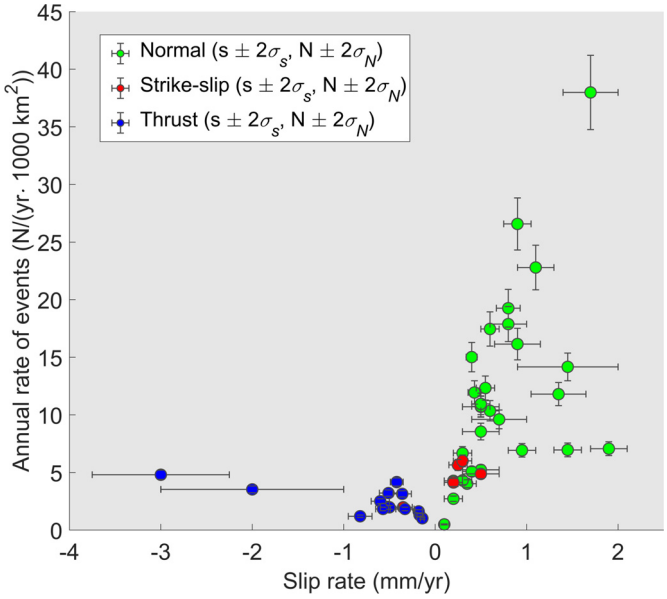

Fig. 8. Scatterplot of the annual rate of earthquakes versus the slip rate during the interseismic phase. Interseismic background normal faults-related events are more frequent than reverse ones analysing areas with similar annual deforming rate. The variable represented at the ordinate axes is calculated by counting the events recorded in the volume surrounding the considered fault. A normalization is then performed with respect to a surface of 1000 km^2. Only earthquakes occurred during the interseismic phase with magnitudes above M_{wc} are taken; data from the INGV earthquake catalogue between 1990 and 2021 are used.

These consequences follow immediately from the classical structural relationships between properties of earthquakes scaling and faulting (Leonard, 2010; Udías et al., 2014; Doglioni et al., 2015a).

In this regard, we also analyzed the features of 47 fault systems in Italy according to the methods discussed in the Supplementary material, Table S3. In Fig. 5 the scatterplot of the lengths of faulting versus the annual slip rate in different tectonic settings is represented. In this picture clearly emerges that extensional faults in Italy are characterized by lower length along strike L_{ext} with

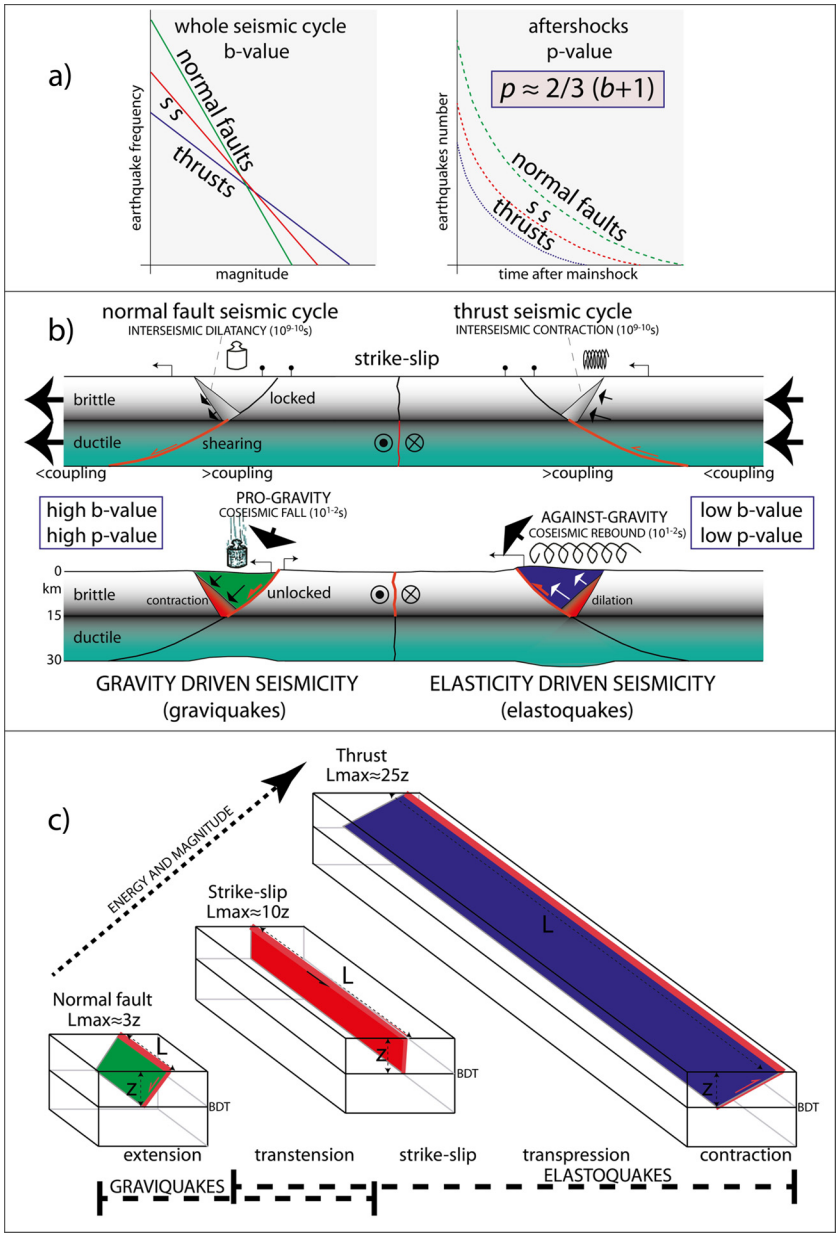

Fig. 9. A recapitulatory diagram of the results discussed in our article. (a) Left panel, the b-value of the Gutenberg–Richter law differs as a function of the tectonic setting, being higher in extensional tectonic settings. Therefore, normal faults have a steeper alignment, which means more low magnitude events and lower maximum magnitude earthquakes with respect to strike-slip (SS) and thrust faults; right panel, being the p-value of the Omori law correlated to the b-value, it shows different aftershocks evolution in time depending on the tectonic settings. On the base of theoretical considerations and statistical analysis of one hundred seismic sequences, the most reliable relationship between them reads $p \approx 2/3\ (b+1)$. Larger p-values mean that seismic dynamics moves more rapidly towards stability, which also implies relatively higher probability of secondary ruptures and more numerous aftershocks than the average reference. (b) A geological interpretation of different scaling behaviors can be given in the light of different contributions to energy balance in the long-term rock volumes mobilization. (c) L_{max} is the average maximum length of the volume and the related adjacent active fault in the different tectonic regimes; z is the seismogenic thickness containing the hypocenter and the aftershocks. The aspect ratio between the two values increases moving from extensional to contractional tectonic settings (modified after Doglioni et al., 2015a and references therein). This is consistent with the larger involved volumes of the great thrust-related earthquakes. The most important tectonic implication of our results provides a possible explanation of the variable length along strike of faults in different dynamic regimes. In extensional tectonic settings the seismogenic volumes are smaller, producing lower maximum magnitudes with respect to the other tectonic settings. Contractional settings require more energy in order to move against gravity and they may involve much larger volumes before reaching the threshold to slip, i.e., producing much larger magnitude events and a lower b-value and p-value.

respect to that of compressive faulting L_{compr} once the average modulus of the slip rate is fixed, as expected. Moreover, in Fig. 6 and Fig. 7 the maximum recorded magnitude versus the annual strain rate and the annual seismic energy rate versus average slip rate are respectively shown. Extensional faulting and compressive tectonic settings are prone to extreme events with similar magnitudes where the deformation rates are the same and they also nucleate equivalent seismic energy expressed in moment magnitude with the same slip rate during interseismic periods in Italy. This implies that rheological, tectonic and topological properties of faulting do not affect significantly the seismic nucleation budget over long timescale. However, Fig. 8, showing the annual rate of earthquakes versus the slip rate during the interseismic phase, proves that the interseismic annual rate of seismic events is higher for extensional tectonic settings in Italy with respect to compressive ones, so that the same geodetic deformation is the reason of different spectra of magnitudes. All these results are coherent with our model.

5. Conclusions

The empirical laws describing the evolution of seismicity over time and its distribution of magnitudes can be derived analytically in a simple way. Omori's law is interpreted as the consequence of a viscous relaxation on a fault plane that progressively removes asperities with decreasing size after a mainshock. The rate of the aftershocks decreases as expected according to the Omori–Utsu law with an exponent p, which is connected to the exponent of the Gutenberg–Richter law b through the relation $p \approx \frac{2}{3}(b+1)$, where the maximum value is reached just after the mainshock. The derivation is correct only if in the relaxation process the seismic contribution dominates the aseismic creep; furthermore, a physical meaning is given to the constants c and z in Eq. (1), usually inferred from experimental data without a theoretical counterpart. The Gutenberg–Richter law, on the other hand, simply reflects the tendency of the Earth's crust to optimize the perturbation triggering power caused by local instabilities. In the other words, fault systems generate the seismic moment necessary for their mechanical stabilization by minimizing the energy required for this purpose. In our model, it is assumed that an initial perturbation can propagate depending on the state of stress and the degree of instability of the rocks surrounding the hypocenter: the fault planes with lower friction allow the spontaneous propagation of both fracture and perturbation; on the contrary barriers suppress it exponentially. In our model, each perturbation has a small probability of growing until it becomes an earthquake of magnitude M_w: there are no energy conditions to constrain its value, which depends on the spatial distribution and physical properties of the barriers and friction variations distribution. Disorder within faults controls the evolution of seismic sequences. In the proposed model, earthquakes occur because of a perturbation triggering nearby seismic events. By imposing that the exponent of the Gutenberg–Richter law has the usually observed value $b \sim 1.0$ at the global scale, averaging all tectonic settings, we obtain that it is related to the coefficient k. It represents the mean triggering capacity of the perturbation during the sequence (or equivalently along the breaking of the single seismic event) from the equation $k = \frac{2}{3}b + 1$, which is why k can be identified with p, and therefore the exponent of the Omori–Utsu law can be simply interpreted as the "propensity to nucleation".

Finally, variations in the coefficients b and p are connected to the different geodynamic and tectonic settings, showing that a relationship between fracturing in the fault zone, value of b, "efficiency" of the seismic process, duration of the seismic sequences and geodynamic environment exists (compare with Fig. 9). Several cases of fault systems in Italy are investigated. We can conclude that seismicity and geology act on each other so that, if certainly seismic events determine the geological features of a region, such as the height of the mountains or the extension of the plains, local tectonics, rock physics and disorder within the fault interface, in turn, shape seismicity, which must be taken into consideration for possible applications in modeling and seismic hazard.

CRediT authorship contribution statement

Davide Zaccagnino tuned the theoretical model and prepared the figures (except for Fig. 9, realized by Carlo Doglioni). Luciano Telesca perfected the model. Davide Zaccagnino, Luciano Telesca and Carlo Doglioni contributed the general idea of the paper. Carlo Doglioni wrote the geological interpretation of the results. All the authors discussed extensively the results and they all reviewed the manuscript.

Declaration of competing interest

The authors declare that they have no known competing financial interests or personal relationships that could have appeared to influence the work reported in this paper.

Acknowledgements

The research was supported by Sapienza University of Rome and by the INGV PhD scholarship awarded to Davide Zaccagnino (November 2021–ongoing). This article has been inspired by the MSc thesis in Theoretical Physics "Near breaking faults" by Davide Zaccagnino, Department of Physics, Sapienza University of Rome, October 2021. We thank the editor Hans Thybo for handling our manuscript and for his precious suggestions which greatly improved our paper. We are grateful to five anonymous reviewers for their comments. Discussions with Andrea Pelissetto, Federico Ricci Tersenghi, Elisa Tinti and Angelo Vulpiani have been constructive and fruitful.

Appendix A. Supplementary material

Supplementary material related to this article can be found online at https://doi.org/10.1016/j.epsl.2022.117511.

References

Aki, K., 1981. A probabilistic synthesis of precursory phenomena. In: Earthquake Prediction: An International Review, vol. 4, pp. 566–574.
Allmann, B.P., Shearer, P.M., 2009. Global variations of stress drop for moderate to large earthquakes. J. Geophys. Res., Solid Earth 114 (B1).
Amato, A., Azzara, R., Chiarabba, C., et al., 1998. The 1997 Umbria-Marche, Italy, earthquake sequence: a first look at the main shocks and aftershocks. Geophys. Res. Lett. 25 (15), 2861–2864.
Bak, P., Tang, C., 1989. Earthquakes as a self-organized critical phenomenon. J. Geophys. Res., Solid Earth 94 (B11), 15635–15637.
Boffetta, G., Carbone, V., Giuliani, P., Veltri, P., Vulpiani, A., 1999. Power laws in solar flares: self-organized criticality or turbulence? Phys. Rev. Lett. 83 (22), 4662.
Brace, W.F., 1960. An extension of the Griffith theory of fracture to rocks. J. Geophys. Res. 65 (10), 3477–3480.
Brune, J.N., 1970. Tectonic stress and the spectra of seismic shear waves from earthquakes. J. Geophys. Res. 75 (26), 4997–5009.
Chelidze, T., Vallianatos, F., Telesca, L. (Eds.), 2018. Complexity of Seismic Time Series: Measurement and Application. Elsevier.
Chiaraluce, L., Di Stefano, R., Tinti, E., et al., 2017. The 2016 central Italy seismic sequence: a first look at the mainshocks, aftershocks, and source models. Seismol. Res. Lett. 88 (3), 757–771.
Cochran, E.S., Vidale, J.E., Tanaka, S., 2004. Earth tides can trigger shallow thrust fault earthquakes. Science 306 (5699), 1164–1166.
Daniel, G., Marsan, D., Bouchon, M., 2008. Earthquake triggering in southern Iceland following the June 2000 Ms 6.6 doublet. J. Geophys. Res., Solid Earth 113 (B5).
Dieterich, J., 1994. A constitutive law for rate of earthquake production and its application to earthquake clustering. J. Geophys. Res. 99, 2601–2618.
Doglioni, C., Carminati, E., Petricca, P., Riguzzi, F., 2015a. Normal fault earthquakes or graviquakes. Sci. Rep. 5 (1), 1–12.
Doglioni, C., Barba, S., Carminati, E., Riguzzi, F., 2015b. Fault on-off versus strain rate and earthquakes energy. Geosci. Front. 6 (2), 265–276.
Gabrielov, A., Keilis-Borok, V., Jackson, D.D., 1996. Geometric incompatibility in a fault system. Proc. Natl. Acad. Sci. 93 (9), 3838–3842.
Goebel, T.H., Kwiatek, G., Becker, T.W., Brodsky, E.E., Dresen, G., 2017. What allows seismic events to grow big?: Insights from b-value and fault roughness analysis in laboratory stick-slip experiments. Geology 45 (9), 815–818.
Goltz, C., 1997. Fractal and chaotic properties of earthquakes. In: Fractal and Chaotic Properties of Earthquakes. Springer, pp. 3–164.
Guo, Z., Ogata, Y., 1997. Statistical relations between the parameters of aftershocks in time, space, and magnitude. J. Geophys. Res., Solid Earth 102 (B2), 2857–2873.
Gulia, L., et al., 2016. Short-term probabilistic earthquake risk assessment considering time-dependent b values. Geophys. Res. Lett. 43 (3), 1100–1108.
Gutenberg, B., Richter, C.F., 1944. Frequency of earthquakes in California. Bull. Seismol. Soc. Am. 34 (4), 185–188.
Helmstetter, A., Shaw, B.E., 2009. Afterslip and aftershocks in the rate-and-state friction law. J. Geophys. Res., Solid Earth 114 (B1).

Helmstetter, A., Sornette, D., 2002. Subcritical and supercritical regimes in epidemic models of earthquake aftershocks. J. Geophys. Res., Solid Earth 107 (B10), ESE-10.
Hirata, T., 1989. A correlation between the b value and the fractal dimension of earthquakes. J. Geophys. Res., Solid Earth 94 (B6), 7507–7514.
ITHACA Working Group, 2019. ITHACA (ITaly HAzard from CApable faulting). A database of active capable faults of the Italian territory. Version December 2019. ISPRA Geological Survey of Italy. Web Portal. http://sgi2.isprambiente.it/ithacaweb/Mappatura.aspx.
Kagan, Y.Y., 1993. Statistics of characteristic earthquakes. Bull. Seismol. Soc. Am. 83 (1), 7–24.
Kagan, Y.Y., Jackson, D.D., 1991. Long-term earthquake clustering. Geophys. J. Int. 104 (1), 117–133.
Leonard, M., 2010. Earthquake fault scaling: self-consistent relating of rupture length, width, average displacement, and moment release. Bull. Seismol. Soc. Am. 100 (5A), 1971–1988.
Nandan, S., Ram, S.K., Ouillon, G., Sornette, D., 2021. Is seismicity operating at a critical point. Phys. Rev. Lett. 126 (12), 128501.
Neely, J.S., Stein, S., 2021. Why do continental normal fault earthquakes have smaller maximum magnitudes? Tectonophysics 809, 228854.
Ogata, Y., 1983. Estimation of the parameters in the modified Omori formula for aftershock frequencies by the maximum likelihood procedure. J. Phys. Earth 31 (2), 115–124.
Petruccelli, A., et al., 2019. The influence of faulting style on the size-distribution of global earthquakes. Earth Planet. Sci. Lett. 527, 115791.
Rovida, A., Locati, M., Camassi, R., Lolli, B., Gasperini, P., 2020. The Italian earthquake catalogue CPTI15. Bull. Earthq. Eng. 18 (7), 2953–2984. https://doi.org/10.1007/s10518-020-00818-y.
Salditch, L., Stein, S., Neely, J., Spencer, B.D., Brooks, E.M., Agnon, A., Liu, M., 2020. Earthquake supercycles and long-term fault memory. Tectonophysics 774, 228289.
Scholz, C.H., Dawers, N.H., Yu, J.-Z., Anders, M.H., Cowie, P.A., 1993. Fault growth and fault scaling laws: preliminary results. J. Geophys. Res. 98, 21951–21961.
Schorlemmer, D., Wiemer, S., Wyss, M., 2005. Variations in earthquake-size distribution across different stress regimes. Nature 437 (7058), 539–542.
Scognamiglio, L., Tinti, E., Michelini, A., et al., 2010. Fast determination of moment tensors and rupture history: what has been learned from the 6 April 2009 L'Aquila earthquake sequence. Seismol. Res. Lett. 81 (6), 892–906.
Shcherbakov, R., 2021. Statistics and forecasting of aftershocks during the 2019 Ridgecrest, California, earthquake sequence. J. Geophys. Res., Solid Earth 126 (2), e2020JB020887.
Stein, S., Geller, R.J., Liu, M., 2012. Why earthquake hazard maps often fail and what to do about it. Tectonophysics 562, 1–25.
Tsallis, C., 1988. Possible generalization of Boltzmann–Gibbs statistics. J. Stat. Phys. 52 (1), 479–487.
Turcotte, D.L., 1989. Fractals in geology and geophysics. Pure Appl. Geophys. 131 (1), 171–196.
Udías, A., Vallina, A.U., Madariaga, R., Buforn, E., 2014. Source Mechanisms of Earthquakes: Theory and Practice. Cambridge University Press.
Utsu, T., 1961. A statistical study on the occurrence of aftershocks. Geophys. Mag. 30, 521–605.
Utsu, T., Ogata, Y., 1995. The centenary of the Omori formula for a decay law of aftershock activity. J. Phys. Earth 43 (1), 1–33.
Valerio, E., Tizzani, P., Carminati, E., Doglioni, C., 2017. Longer aftershocks duration in extensional tectonic settings. Sci. Rep. 7 (1), 1–12.
Ventura, G., Di Giovambattista, R., 2013. Fluid pressure, stress field and propagation style of coalescing thrusts from the analysis of the 20 May 2012 ML 5.9 Emilia earthquake (Northern Apennines, Italy). Terra Nova 25 (1), 72–78.
Wang, J.H., 1994. On the correlation of observed Gutenberg–Richter's b value and Omori's p value for aftershocks. Bull. Seismol. Soc. Am. 84 (6), 2008–2011.
Wells, D.L., Coppersmith, K.J., 1994. New empirical relationships among magnitude, rupture length, rupture width, rupture area, and surface displacement. Bull. Seismol. Soc. Am. 84 (4), 974–1002.
Zaccagnino, D., Telesca, L., Doglioni, C., 2021. Different fault response to stress during the seismic cycle. Appl. Sci. 11 (20), 9596.
Zaccagnino, D., Vespe, F., Doglioni, C., 2020. Tidal modulation of plate motions. Earth-Sci. Rev. 205, 103179.